Available online at www.sciencedirect.com

ScienceDirect

journal homepage: www.elsevier.com/locate/he

Kinetics of hydrogen evolution reaction on nickel modified by spontaneous Ru deposition: A rotating disk electrode and impedance spectroscopy approach

Esteban A. Franceschini [a,*], *Gabriela I. Lacconi* [b], *Horacio R. Corti* [a,c]

[a] *Departamento de Física de la Materia Condensada, Centro Atómico Constituyentes, Comisión Nacional de Energía Atómica, Av. Gral. Paz 1499 (B1650KNA) San Martín, Buenos Aires, Argentina*

[b] *INFIQC-CONICET, Dto. de Fisicoquímica – Facultad de Ciencias Químicas, Universidad Nacional de Córdoba, Ciudad Universitaria, 5000, Córdoba, Argentina*

[c] *Departamento de Química Inorgánica, Analítica y Química Física and INQUIMAE-CONICET, Facultad de Ciencias Exactas y Naturales, Universidad de Buenos Aires, Ciudad Universitaria, Pabellón II, C1428EHA, Buenos Aires, Argentina*

ARTICLE INFO

Article history:
Received 14 August 2015
Received in revised form
20 December 2015
Accepted 22 December 2015
Available online 19 January 2016

Keywords:
Hydrogen generation
Nickel/ruthenium
Spontaneous deposition
Rotating disk electrode
Impedance spectroscopy

ABSTRACT

The kinetics of hydrogen evolution reaction (HER) was studied on nickel catalysts prepared using a ruthenium spontaneous deposition method. Rotating disk electrode (RDE) and electrochemical impedance spectroscopy (EIS) were used for electrochemical characterization, and the results of the analysis were compared with pure nickel catalysts. Three different deposition times were used to obtain different ruthenium loads and to analyze their impact on the electrocatalytic activity. Kinetic and thermodynamic parameters of the reaction were obtained for freshly synthesized catalysts, and also for catalysts aged using a short chronoamperometric procedure. The presence of ruthenium was found to shift the reaction onset potential up to about 160 mV to lower overpotentials comparing with pure nickel, which not increases after ageing, showing a substantial improvement in catalytic activity. Results of Tafel and Koutecky–Levich (K–L) analysis have shown that the HER rate determining step is the Volmer reaction with Langmuir type adsorption for both, Ni/Ru fresh and aged catalysts.

Introduction

Nickel metal is widely used as cathode in alkaline electrolyzers because of its corrosion resistance at high pH values [1–6]. Besides, several studies have shown that nickel electroactivity towards the hydrogen evolution reaction (HER), decreases due to the formation of hydrides under cathodic potentials [7–9].

* *Corresponding author*. Tel.: +5411 6772 7189; fax: +5411 6772 7121.
E-mail address: efrances@tandar.cnea.gov.ar (E.A. Franceschini).

http://dx.doi.org/10.1016/j.ijhydene.2015.12.143

The mechanism of HER in alkaline solution is usually modeled as occurring through a three steps mechanisms. Two of them are electrochemical (Tafel and Heyrovsky reactions) while the third one is a surface adsorption process (Tafel reaction) [10–12]:

$$Ni + H_2O + e^- \underset{k_{-V}}{\overset{k_V}{\rightleftharpoons}} Ni\cdots H_{ad} + \underset{(Volmer\ Reaction)}{HO^-}$$

$$2Ni\cdots H_{ad} \underset{k_{-T}}{\overset{k_T}{\rightleftharpoons}} 2Ni + \underset{(Tafel\ Reaction)}{H_2}$$

$$Ni\cdots H_{ad} + H_2O + e^- \underset{k_{-H}}{\overset{k_H}{\rightleftharpoons}} Ni + HO^- + \underset{(Heyrovsky\ Reaction)}{H_2}$$

Nickel based bimetallic catalysts, such as Ni/Fe [13], Ni/W [14], Ni/Ir [15], Ni/Co [16], Ni/Ag [17], Ni/Cu [18], Ni/Mn [19], and Ni/Ce [20], usually obtained by electrodeposition, have been widely studied in recent years in the search for catalysts that improve the activity of nickel towards the HER, and prevent its deactivation by formation of hydrides. Houlachi and coworkers [21]. have recently reviewed the main features of HER in bimetallic catalysts.

Oxides and hydroxides are easily formed on the ruthenium surface due to the discharge of water [22–25] and, because Ru is less expensive than other metals such as Ir, Pt or Pd, it is widely used as an activator in electrocatalysis.

Several studies have demonstrated that the HER electrocatalytic activity of Ni can be substantially enhanced by deposition of RuO_2 thin layers, either by direct thermal decomposition of $RuCl_3$ solutions [26], or by electrodeposition of RuO_2 particles from a Ni/Ru bath [27,28]. In all cases, activation of electrodes is observed but, the low mechanical stability of the catalysts and the high costs of the process prevent its practical application.

In recent years, the synthesis of catalysts via spontaneous deposition has been proposed as a fast and simple way for the synthesis of modified nickel electrodes [29–33]. This method has the additional advantage of allowing the activation of the electrodes without disassembling the electrolyzer.

In situ Ni activation by Ru electrodeposition during H_2 evolution in 40% KOH at 120 °C was reported by Schmidt et al. [34]. Furthermore, Wieckowski and co-workers [35–37] have shown that Ru can be spontaneously deposited on Pt from an acidic solution. The possibility of spontaneous deposition of Ru on Ni electrodes has been proposed and investigated by different groups in the last decade. Trasatti and coworkers [38] analyzed the spontaneous deposition of Ru carried out in HCl + $RuCl_3$ solutions. Ru deposition was confirmed by EDX and XPS, and monitored as a function of the deposition time by cyclic voltammetry in 1 M KOH. Ni activation by Ru was verified by the appearance of H adsorption peaks in the voltammetric curve. Musiani and coworkers [39,40], synthesized porous modified Ni deposits by immersing Ni in acid deaerated solutions containing Ru(III) or Ir(IV) chloride complexes. Data showed that the initial large area of the porous nickel deposits was increased after the immersion, and significant differences on the Ru and Ir deposits were observed besides the thickness of the deposit, the oxidation of Ni and the growth of hydrous surface oxides. The catalytic activity of the electrodes modified with noble metals generally improves upon potential cycling, which oxidized Ni and induces the growth of hydrous surface oxides on both, Ru and Ir.

In a previous work we have analyzed the electrochemical behavior of freshly polished nickel electrodes (Ni_f) and nickel electrodes after a short chronoamperometric ageing procedure (Ni_{pc}), using the rotating disk electrode and electrochemical impedance techniques [41]. Based on the kinetic and thermodynamic parameters of the HER in alkaline aqueous solution, we concluded that it occurs through reduction of water, and the Volmer reaction is not controlled by the water diffusion, which is in excess, but by the diffusion of HO^- ions. Thus, a theoretical Koutechy–Levich (K–L) slope, that allows the proper fit of the experimental data, was calculated. Large changes in the electrocatalytic behavior of nickel after the chronoamperometric pulse were observed and correlated with changes in the hydrogen adsorption rate on the catalyst surface. Tafel and K–L analysis show that the rate determining step on Ni_f is a one electron transfer process (Volmer reaction), showing a Langmuir type H adsorption isotherm, while on Ni_{pc} the number of transferred electrons decreases, becomes temperature dependent, and the H adsorption isotherm is Temkin type.

In this work, nickel/ruthenium catalysts were synthesized via spontaneous deposition and electrochemically characterized. The ruthenium deposition time was modified in order to obtain different loads. The modified nickel electrodes were analyzed in alkaline solution by linear sweep voltammetry at different rotation rates and temperatures, cyclic voltammetry, electrochemical impedance spectroscopy (EIS), and chronoamperometry.

Although similar catalysts to those prepared in this work have been reported in the literature, the kinetic and thermodynamic values necessary for the proper understanding of the parameters that affect the catalytic activity of these materials have not been measured. In this work the KL slopes were calculated on the basis of the HER mechanism in alkaline solution presented in a previous work [41], and used to establish changes in the reaction mechanism with temperature and ageing for all the catalysts synthesized. Conway and Tafel analysis were conducted in order to analyze the processes occurring on the electrodes surfaces, as hydrogen adsorption. The KL slopes have not been reported in previous works, nor activation energy, activation enthropy and enthalpy values (a_S and $a_{H,}$ respectively), for this type of catalyst. The analysis of these parameters, determined in this work, are necessary for the proper understanding of the mechanism by which the nickel is activated towards the HER by adding ruthenium and allows us to establish which is the effect of the adding of ruthenium on the catalytic activity of nickel based catalysts, fresh and after a short ageing process.

Experimental

Chemicals

Potassium hydroxide (Anedra RA reagent), hydrochloric acid 36.5–37% (Cicarelli, PA grade), ethanol 96% (Cicarelli) and ruthenium trichloride (99.99%, Aldrich) were used as received. All aqueous solutions were prepared with Milli-Q water, degassed using high purity N_2 (Indura S.A.).

Catalyst preparation

The nickel electrodes (99.9 purity) for catalysts synthesis (area = 0.196 cm^2) were mechanically polished with 0.05 μm alumina. The electrodes were repeatedly cleaned with ethanol and by consecutive immersion steps in 1 M KOH, and HCl (10% w/w) aqueous solutions, during 1 min, in order to degrease the surface. The catalysts preparation via spontaneous deposition was conducted by immersion of freshly polished nickel electrodes in deaerated $RuCl_3$ solution (1 g dm^{-3}), at room temperature. Three deposition time were used in order to obtain different ruthenium loads on the nickel surface. All catalysts were synthesized using freshly prepared $RuCl_3$ solutions to prevent changes in the concentration of the solution for the repeated uses.

Electrochemical characterization

All the electrochemical experiments were conducted in a conventional three-electrode electrochemical cell with a thermostatic jacket. A platinum sheet was used as counter electrode and a saturated calomel electrode (SCE) as reference electrode (0.243 V *vs*. RHE). The reference electrode was kept outside the cell to maintain it at room temperature and the circuit was closed using a capillary filled with KCl in agar. 1 M KOH aqueous solution was used as electrolyte. During all the electrochemical measurements, a nitrogen flux was maintained over the electrolyte surface to properly deaerate the solution.

The electrochemical studies were performed with an Autolab PGStat30 potentiostat/galvanostat with FRA2 module, coupled to a rotating disk electrode (Pine Research Inst.; Raleigh, NC). RDE measurements were conducted on a massive Ni disk electrode mounted in an interchangeable RDE holder (Pine Research Inst.; Raleigh, NC), and the rotation rate was varied between 100 and 2500 rpm. The uncompensated ohmic electrolyte resistance (~50 Ω) was measured via high frequency ac impedance in N_2 saturated 1 M KOH solution, and used to calculate the cell constant. Ohmic drop correction to the applied potentials was made automatically by Autolab software (Metrohm Autolab Nova 1.10). The temperature of the cell during the experiments was controlled using a Lauda Alpha RA 8 controller, and the measurements were conducted between 278 K and 308 K, in steps of 5 K. The area used for all current densities calculation was the corresponding to the geometric area of the disk electrode (0.196 cm^2).

Cyclic voltammetry (CV) and linear sweep voltammetry (LSV) experiments were conducted between 0.1 and −1.5 V (*vs*. SCE) at a scan rate of 10 mV s^{-1} for all nickel electrodes.

Impedance spectroscopy experiments were carried out by applying a 10 mV potential modulation at frequencies between 10 mHz and 100 kHz at different electrode potentials, such as: open circuit potential (OCP), HER onset potential, 0.1 V and 0.3 V more cathodic than the corresponding onset potential of each catalyst. These selected potential values were chosen in order to cover the potential range where the HER takes place [42]. The fitting of the measured data were carried out using the ZView 3.3 program (Scribner Associates, Inc.) in the frequencies interval of 10 mHz and 100 kHz with the equivalent circuit proposed by Armstrong and Henderson [43].

Chronoamperometric measurements were carried out applying a potential pulse at −1.5 V (*vs*. SCE) during 4 h at 298 K. A 900 rpm electrode rotation rate was used for the EIS and chronoamperometric experiments, in order to prevent the formation of bubbles.

Electrochemical analysis

The HER overall current density (j) can be expressed in terms of the kinetic current density, j_k, and the boundary-layer diffusion limited current density, j_d by the Koutecky–Levich (K–L) equation [44]:

$$\frac{1}{j} = \frac{1}{j_k} + \frac{1}{j_d} = \frac{1}{j_k} + \frac{1}{B\omega^{1/2}} \tag{1}$$

where ω is the rotation rate (rpm) and B is the Levich slope given by,

$$B = 0.2nFC_oD_o^{2/3}\nu^{-1/6} \tag{2}$$

where 0.2 is a constant used when ω is expressed in rpm, n is the number of electrons transferred per molecule of H_2O reduced, F the Faraday constant (96,485 C mol^{-1}), C_O is the HO^- concentration in the solution (0.001 mol cm^{-3}), D_O is the HO^- diffusion coefficient (5.3×10^{-5} cm^2 s^{-1}) [45], and ν the kinematic viscosity of the 1 M KOH solution (9.473×10^{-3} cm^2 s^{-1}) [45]. The theoretical value of B^{-1} for single electron charge transfer (i.e.,n = 1) process is 1.689×10^{-2} mA^{-1} $cm^2 \cdot rpm^{1/2}$ [41]. The comparison of the calculated slope for the straight lines in the K–L plots with the theoretical B value allows evaluating the number of electrons involved in the reaction.

The Tafel equation is:

$$\log j_k = \frac{2.3RT}{nF\alpha}E + j_o = bE + j_o \tag{3}$$

where j_0 is the exchange current, b is the Tafel slope parameter, n is the number of electrons transferred, and α is the transfer coefficient. In order to calculate the value of n, we used $\alpha = 0.5$. The kinetic current density (j_k), was calculated by correcting the measured current density (j) by the mass transfer using the diffusional limiting current (j_d), with Eq. (4):

$$j_k = j\frac{j_d}{(j_d - j)} \tag{4}$$

Usually, it is observed that when b is independent of temperature, the transfer coefficient shows a linear dependence with temperature. The α parameter is composed of enthalpic (α_H) and entropic (α_S) contributions. The terms α_H and α_S are related to the change of the electrochemical enthalpy of activation and the entropy of activation with the electrode potential, respectively [41,46]. They can be calculated employing the Conway analysis by a linear fit of the 1/b *vs*. 1/T plot, and using the Eq. (5).

$$\frac{1}{b} = \frac{n\alpha_H F}{2.303RT} + \frac{n\alpha_S F}{2.303R} \tag{5}$$

Finally, it is possible to calculate the apparent activation energy ($\Delta H^{\#}$) using the j_0 values, calculated with the Tafel, and the Arrhenius equations:

$$\Delta H^{\#} = -R\left[\frac{d\ln j_o}{j(1/T)}\right] \quad (6)$$

Structural characterization

Scanning electron images were obtained using a Supra 40 (Zeiss Company) FESEM operating at 3 kV, equipped with EDX. EDX spectra and EDX mapping were obtained operating at 6 kV.

X-ray diffractograms were recorded employing the Cu Kα radiation (λ = 1.5406 Å), using a PANalytical X'Pert PRO diffractometer (40 kV, 40 mA), in the θ − 2θ Bragg–Brentano geometry at room temperature. A 2θ range between 10° and 70° was selected, with increments of 0.02° and a counting time of 14 s per step. The FULLPROF program [47] was applied to refine the crystal structure by Rietveld method. A pseudo-Voigt shape function was used to fit the experimental data. The data refined were atomic positions, lattice parameters, peak shape, isotropic thermal parameters, and occupation factors.

Results and discussion

Catalyst synthesis

Three NiRu catalysts were synthesized with 500 s deposition (NR500), 1800 s deposition (NR1800), and 3600 s deposition (NR3600).

In order to study the deposition process, the open circuit potential (OCP) was monitored during the spontaneous deposition of ruthenium. Fig. 1 shows the variation of OCP vs. deposition time for the NR500 catalyst. It can be observed that initially OCP is negative, that is consistent with a displacement reaction [48], followed by a change on the electrode potential to positive values, reaching ~0.2 V (vs SCE), which is almost time independent. The change in the electrode OCP is due to changes in the electrode surface, and the OCP profile indicates that the immersion nickel process involves two different steps, the nucleation and growth of Ru on the surface

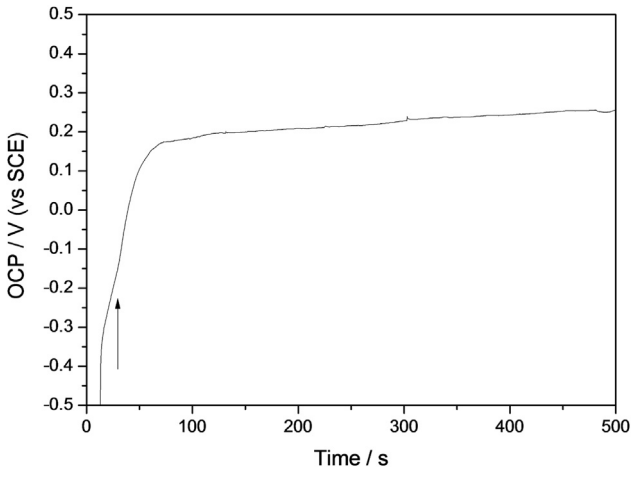

Fig. 1 – OCP as a function of time for a Ni_f sample immersed in 1 g dm^{-3} $RuCl_3$ solution.

[49,50]. A shoulder coupled to the OCP decay (showed with an arrow in Fig. 1) is observed at around 30 s. That shoulder is similar to that observed for the electrochemical nucleation/growth of nanoparticles over a surface [17] being indicative of the particles formation on the nickel surface [51–53]. Stabilization of the OCP values is reached after 75 s.

Structural characterization

Scanning electron micrographs were obtained in order to analyze changes in the structure, and the presence of crevices with the deposition time. In Fig. 2a the SEM micrographs of NR500, NR1800 and NR3600 electrodes at a magnification of 100.000 x are presented. The samples are mainly granular, show polishing marks, and superficial fractures or crevices were not observed.

In Fig. 2b, the X-ray diffraction (XRD) pattern of the $NR1800_f$ sample is presented. The XRD patterns for all the Nickel/Ruthenium catalysts clearly exhibits the characteristic reflections expected for nickel with face centered cubic (fcc) structure [23]. All samples show peaks at 44.6° and 65.0°, corresponding to aluminum present in the sample holder. Ru peaks are masked by the Ni peaks with much higher intensity. The low intensity of the ruthenium peaks is due to the fact that ruthenium is found only on the catalyst surface. The intensities ratio of the XRD peaks of Ni (1 1 1) and Ni (2 0 0) planes is 6.72, showing a preferential (1 1 1) plane, similar to the observed in the freshly polished nickel catalyst. The values of 2θ for the Ni (1 1 1) and (2 0 0) planes are 44.5° (FWHM = 0.192°) and 51.8° (FWHM = 0.288°), respectively; with a d-spacing distance of 2.03 Å, for the plane (1 1 1) and 1.76, for the (2 0 0) plane.

EDX spectra (Fig. 3a) show the typical Ni Lα band (0.851 keV). Although the Ru Lα band at 2.558 keV (Fig. 3b) can also be detected, it is much less intense than the Ni signals. This is due to the fact that EDX beam has high penetration in the material and ruthenium is deposited only on the material surface, which makes very difficult its quantification. However, it is observed an almost linear relationship between the Ru Lα band area and the deposition time (Fig. 3c), indicating an increase in the proportion of Ru in the catalyst surface.

EDX mapping shows that the composition is homogeneous in the entire sample surface, and only traces of Al and Si (from the polishing alumina) contaminate the surface.

Cyclic voltammetry and chronoamperometric analysis

Freshly synthesized catalysts

Fig. 4 shows typical cyclic voltammograms of freshly polished bare nickel and the three Ni/Ru synthesized catalysts, measured at 298 K and a scan rate of 10 mV s^{-1} in 1 M KOH solution.

A decrease in the onset potential for the HER was observed in the catalyst synthesized when the ruthenium deposition times were 500 and 1800 s. The lowest onset potential corresponds to the $NR1800_f$ catalyst, with a current density measured at 1.5 V (*vs.* SCE) almost 5 times larger than that for bare Ni_f [41]. The progressive activation of nickel by ruthenium deposition could be originated from a diminution of the Fermi level of nickel [54,55]. With a

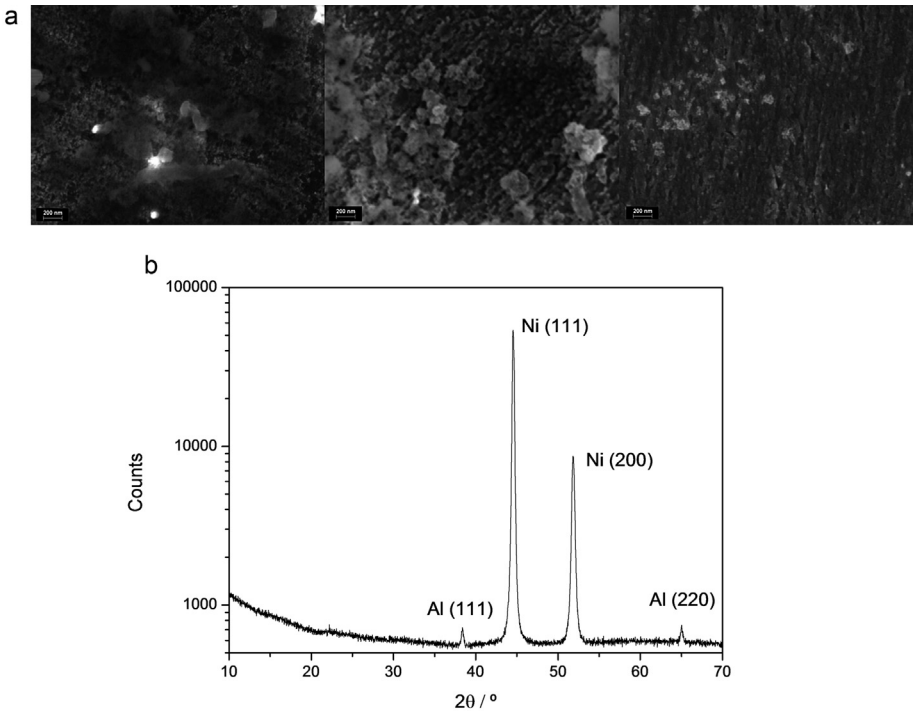

Fig. 2 – a: SEM micrographs of fresh NR500 (left), NR1800 (middle) and NR3600 (right) catalysts measured at 6 keV and a magnification of 100.000 x, respectively. b: X-ray diffraction pattern of NR1800$_f$.

deposition time of 3600 s (NR3600), the electrochemical activity towards the HER is notoriously reduced, probably as a consequence of an excess of ruthenium (and ruthenium oxides) on the surface. It is well known that ruthenium is easily oxidized in water, and ruthenium oxides have very low electroactivity towards HER [56]. Additionally, an excess of ruthenium content would prevent the H atoms to reach the nickel surface. In the inset of Fig. 4, the changes in the

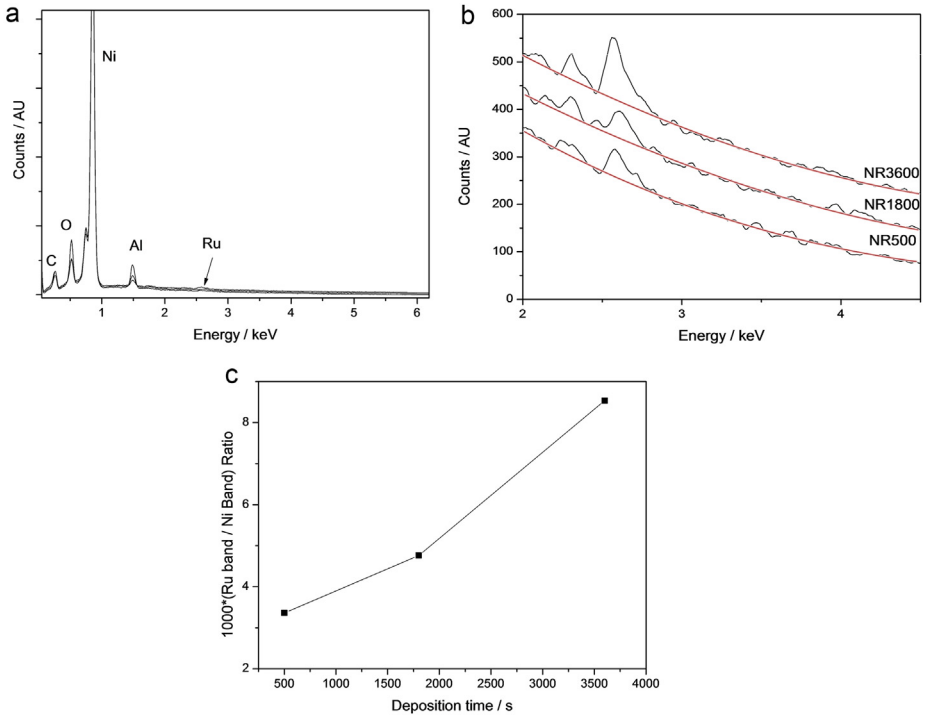

Fig. 3 – a: EDX spectrum of NR1800$_f$ measured at 6 keV. b. Magnification of the EDX spectra of Lα Ru band of NR500, NR1800 and NR3600 catalysts. c. Correlation between deposition time and (Lα Ru band/Lα Ni band) ratio.

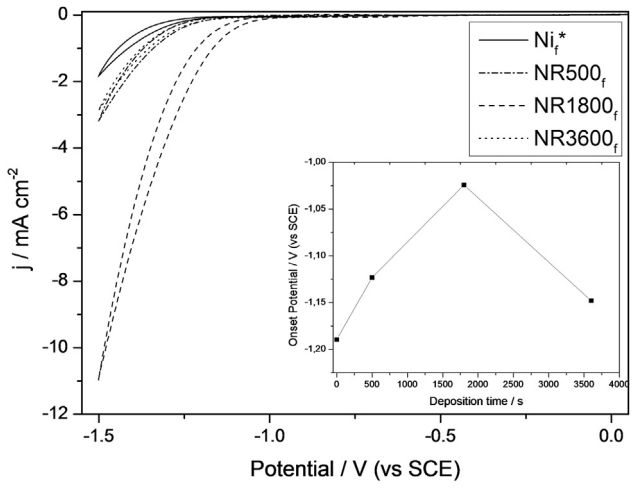

Fig. 4 – Cyclic voltammograms of Ni$_f$ [41], NR500$_f$, NR1800$_f$ and NR3600$_f$ catalysts in 1 M KOH at 298 K (scan rate: 10 mV s^{-1}). Insert: Changes of catalysts onset potential with Ru deposition time.

onset potential with the ruthenium deposition time are showed. It can be seen that deposition during 1800 s, decreases up to 160 mV the OCP of HER compared to that of freshly polished bare nickel (Ni$_f$) [41].

Fig. 5 shows a magnification of the cyclic voltammograms of Ni$_f$ and NR1800$_f$. It is observed that the cathodic (I_c) and anodic (I_a) peaks (marked with arrows in Fig. 5) are separated around 80 mV, and there is a significant increase of the intensity in the presence of ruthenium. I_c and I_a peaks corresponds to the reversible electrosorption of H on Ru [38]. Moreover, the I_a peak in Ni$_f$ is practically absent, while in the nickel ruthenium catalysts, the H adsorption/desorption processes are more reversible, indicating that, unlike it was observed in bare Ni [9], stable nickel hydrides generation is electrochemically disfavored by the presence of ruthenium, avoiding the electrode deactivation.

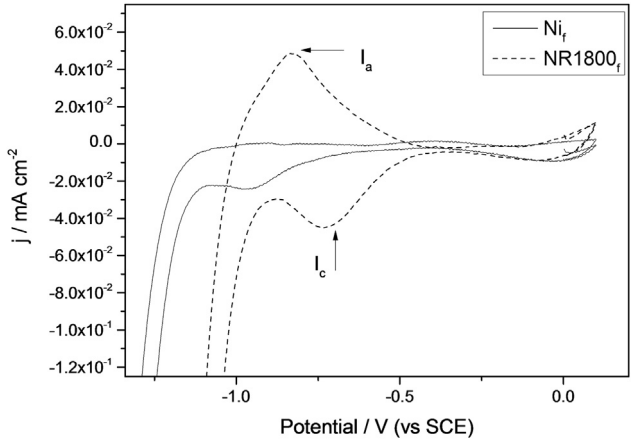

Fig. 5 – Magnification of the cyclic voltammograms shown in Fig. 4.

Short aged catalysts

The Ni/Ru electrodes, after being characterized for different electrochemical techniques (LSV by RDE at different temperatures, EIS at different potentials), were subjected to a chronoamperometric pulse for 4 h, in order to analyze short-term ageing effect of the catalysts during the hydrogen evolution.

Fig. 6 shows the 4 h chronoamperometric profile of the Ni/Ru catalysts synthesized, along with the results for bare nickel measured in a previous work [41]. Two zones can be clearly individualized in the NR500 and NR1800 catalysts, as in Ni electrodes. The first one (between 0 and 100 s), where the current decreases rapidly, and the second one, for t > 100 s, where a gradual increase of the hydrogen generation current was observed, which is due to the catalyst activation. It was previously reported that RuO_2 is a poor catalyst for hydrogen reactions in the as-grown state, but its activity increases after cathodic polarization, due to the formation of metallic ruthenium sites with high electrocatalytic activity [56].

The chronoamperometric current recorded at 4 h in NR1800 is 7.2 times higher than in bare Ni, showing a clear activation of the $NiOH_{ads}$ formation process, induced by the presence of ruthenium in the surface. On the other hand, the NR3600 catalyst shows a different behavior when compared with other catalysts (including bare Ni) at times lower than 100 s. The activation process is much lower for NR3600, and the $NiOH_{ads}$ formation current after the initial decay increases only 1.88 times compared to the initial value, while the corresponding incremental ratios are 2.72 on NR1800 (similar to the observed in NR500) and 3.07 on bare Ni. The observed differences for the water discharge and the HER activation indicates a compromise situation between the amount of deposited ruthenium (and consequently the deposition time) and the current densities obtained.

In Fig. 7 the linear sweep voltammetry of NR1800 catalyst before (NR1800$_f$) and after (NR1800$_{pc}$) the chronoamperometry experiment, are shown. A noticeable increase in the current density at −1.5 V (vs. SCE) is observed after ageing. The NR1800$_{pc}$ catalyst is 6.8 times more active towards the HER than the NR1800$_f$ catalyst. This trend is opposite to that

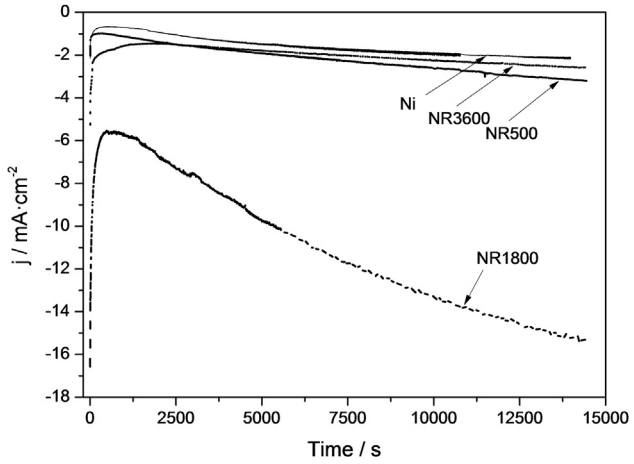

Fig. 6 – Chronoamperometric profile of hydrogen evolution reaction on Ni$_f$ [41], NR500$_f$, NR1800$_f$ and NR3600$_f$ in 1 M KOH obtained at −1.5 V (*vs.* SCE), 298 K, and rotation speed of 900 rpm.

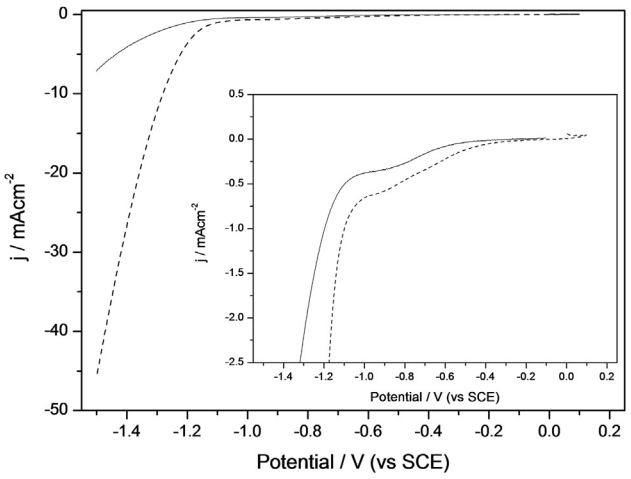

Fig. 7 – LSV of NR1800$_f$ (filled line) and NR1800$_{pc}$ (dashed line) electrodes in 1 M KOH measured at 298 K (scan rate 10 mVs^{-1}). Insert: Magnification of the NR1800$_f$ and NR1800$_{pc}$ LSV.

observed in pure nickel, where after 4 h potential pulse, the current density of Ni$_{pc}$ is 5.6 times lower than that found in Ni$_f$ [41]. In the insert of Fig. 7, it can be seen that HER onset potential is not modified by the ageing process, unlike that is observed in pure nickel where the potential is shifted to higher onset potentials about 0.3 V [41]. Furthermore, the HO^- adsorption current on the NR1800$_{pc}$ surface is 1.75 times higher than the observed in NR1800$_f$ (at −1.0 V (vs. SCE)), indicating an activation of the adsorption process.

For the catalyst NR500 a slight increase in onset potential after ageing is observed, while the catalyst NR3600 exhibits the same onset potential after the ageing process.

RDE analysis

Fig. 8 shows a set of RDE current density–potential curves obtained for NR1800$_f$ and NR1800$_{pc}$ catalysts in N_2 saturated 1 M KOH electrolyte at 298 K.

All catalysts show a well-defined charge transfer kinetic control at potentials above −0.50 (*vs.* SCE) and a mixed kinetic diffusion control, occurring between −0.86 and −0.50 V (*vs.* SCE). In this zone of potential, the nickel oxides reduction and the adsorption of water on the catalysts surface to form nickel hydroxide occurs, related mainly with the Volmer reaction [9].

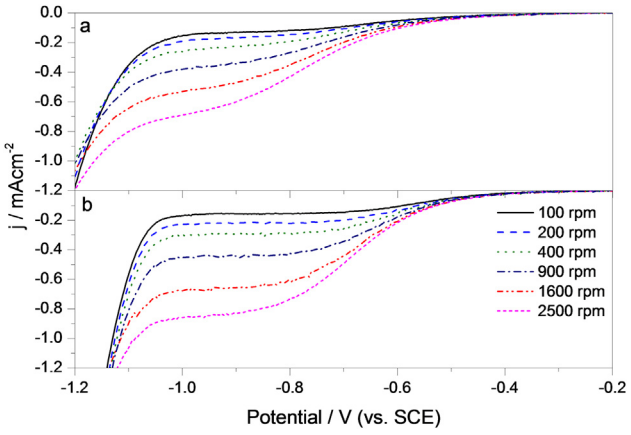

Fig. 8 – RDE curves for HER obtained in 1 M KOH at 298 K on: a) NR1800$_f$; b) NR1800$_{pc}$, at different rotation rates.

It can be seen that while there is no change in the onset potentials, NR1800$_{pc}$ sample has a better defined diffusional control area (between −0.86 and −1.03 V (vs. SCE)), indicating that the electrode was stabilized during the ageing treatment [41].

Fig. 9 shows the Koutecky–Levich plots obtained for NR500 and NR1800 at different potentials, before and after the chronoamperometry, compared to the theoretical curve for one electron transference (dashed line). The linearity of the plot indicates that H_2 evolution is a first order reaction and a noticeable change in j_k (obtained from the $\omega^{-1/2} = 0$ interception) is observed [57]. It is observed that freshly catalysts show an increase in the electron transfer rate with increasing overpotential, whereas in the catalysts after the chronoamperometry, substantially constant j_k values (with overpotential) were observed, indicating a rapid electron transfer [57].

The obtained values of Levich slope (B) and transferred electrons number (n) are summarized in Table 1. It is observed that, in most cases, $n < 1$ ($0.72 < n < 0.94$) indicating that the rate limiting step is the Volmer reaction.

After the chronoamperometry, the transferred electron number increases between 25 and 30% for NR500 and NR1800 catalysts, suggesting a major contribution of the Volmer reaction to the overall reaction when the catalyst is subjected to short-term ageing. On the other hand, in NR3600 catalyst the change in *n* is more dramatic, indicating a change in the reaction mechanism, probably associated to an important contribution of the Heyrovsky reaction.

The mass transfer corrected Tafel plots for the nickel/ruthenium synthesized catalysts before (Fig. 10a) and after (Fig. 10b) the chronoamperometry shows a shift in the equilibrium potentials for all the catalysts. In Fig. 10a (freshly synthesized catalysts) it can be seen that the equilibrium potentials shift to more positive potentials, with respect to pure

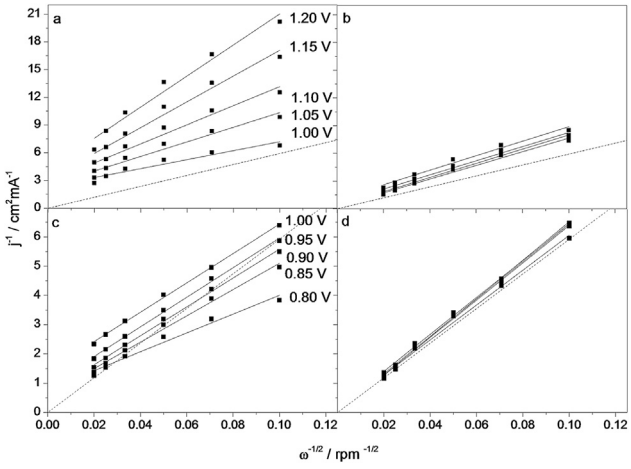

Fig. 9 – K–L plots for HER at 298 K on a) NR500$_f$, b) NR500$_{pc}$, c) NR1800$_f$ and d) NR1800$_{pc}$ at different electrode potentials. The theoretical one electron slope is showed as a dashed line.

Table 1 – Kinetics parameters for the HER on the synthesized catalysts in 1 M KOH calculated from the K–L analysis, Conway analysis (average of the entire range of rotation rates), Tafel slope (average of the values obtained between 278 and 308 K. Rotation rate: 900 rpm) and apparent activation energies for all catalysts.

	b ($V dec^{-1}$)	n	α_H	α_S (K^{-1})	j_0 ($mA\ cm^{-2}$)	Ea ($kJ\ mol^{-1}$)
$NR500_f$	−0.137	0.72	-2.94×10^{-4}	-1.36×10^{-4}	7.85×10^{-5}	48.8
$NR500_{pc}$	−0.127	0.94	-8.85×10^{-4}	-5.16×10^{-4}	3.11×10^{-5}	38.2
$NR1800_f$	−0.131	0.61	-1.93×10^{-3}	-5.81×10^{-5}	3.61×10^{-4}	39.0
$NR1800_{pc}$	−0.131	0.82	-3.24×10^{-3}	-4.87×10^{-5}	1.05×10^{-4}	19.3
$NR3600_f$	−0.131	0.75	-3.64×10^{-4}	-6.62×10^{-4}	4.16×10^{-4}	28.9
$NR3600_{pc}$	−0.150	1.45	-1.28×10^{-3}	-3.11×10^{-4}	5.75×10^{-5}	27.6
Ni_f [41]	–	–	-1.13×10^{-3}	3.11×10^{-3}	8.02×10^{-5}	60.3
Ni_{pc} [41]	–	–	-9.92×10^{-4}	2.11×10^{-3}	1.76×10^{-7}	65.3

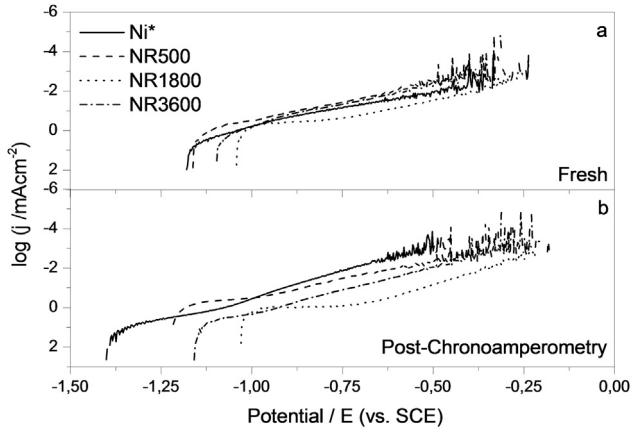

Fig. 10 – Mass transfer corrected Tafel plots for the HER on a) fresh catalysts and b) catalysts subjected to four hour chronoamperometry at 1600 rpm and 293 K. Scan rate = 10 mV s^{-1}. * Ref. [41].

nickel, by adding ruthenium. Besides, nickel/ruthenium catalysts, before and after ageing treatment, show the same equilibrium potential, while the pure nickel catalyst after chronoamperometry shows a shift to higher overpotentials.

Tafel slope (average of the entire range of temperatures used, see Table 1) is similar, around −0.130 V dec^{-1}, for all the catalysts, except the NR3600 catalyst whose values change from −0.131 V dec^{-1} to −0.150 V·dec^{-1} after chronoamperometry, indicating a change in the reaction mechanism. Conway graphics (not shown) were done using the reciprocal of Tafel slopes versus 1/T obtained for each catalyst [41,58], and the respective values of α_H and α_S, calculated using equation (5), are presented in Table 1.

Thus, for NR500 and NR3600 catalysts the entropic component is the major contribution during reaction activation, similar to that observed with pure nickel [41]. On the other hand, for NR1800 catalyst the enthalpic contribution to activation seems to overcome the entropic contribution. This indicates that, for NR1800, the enthalpic change with temperature in the activation energy is the main factor controlling the reaction kinetic at a given electrode potential.

The α_H and α_S values obtained for all nickel/ruthenium catalysts are lower than those previously observed in pure nickel [41], except for the enthalpic component in the NR1800 catalyst both, fresh and aged. The negative α_H values indicate a positive heat of adsorption. All nickel/ruthenium catalysts exhibit a negative α_S, unlike what is observed in pure nickel where α_S is positive. The negative sign of α_S, indicates that during activation the system is ordered, suggesting a greater Volmer reaction contribution to the overall process, since this reaction is the only of the three (Volmer, Tafel and Heyrovsky) having an ordering effect on the system. This value of α_S is probably related with the facility of Ru atoms to adsorb water molecules [59,60]. In the case of NR1800 catalysts, the preponderance of the enthalpy component over the entropic component, with α_H values even higher than those found in pure nickel, indicates that the adsorption is favored in comparison to the other catalysts, which could explain the higher catalytic activities presented by the NR1800 catalyst. Particularly, α_H for the catalyst NR1800 grows almost 70% after ageing, showing an increased tendency to adsorb water on the catalyst surface.

The values of exchange current for each catalyst shown in Table 1 (average over the whole range of temperatures, between 278 and 308 K), are in most of the cases, higher than those found for pure Ni, as summarized in Table 1.

$NR500_f$ catalyst has similar j_0 to that obtained for Ni_f, while the $NR500_{pc}$ catalyst presents only a slight decrease from $NR500_f$ (with a j_0 two magnitude orders higher than Ni_{pc} catalyst), showing a substantial improvement over the performance of the nickel pure catalyst. Moreover, the NR1800 catalyst has a higher current density than NR500 and NR3600.

The apparent activation energies ($\Delta H^{\#}$) for each of the catalysts were calculated using the temperature dependence of j_0, and eqn (6). The values of $\Delta H^{\#}$ for all catalysts are summarized in Table. It is observed that the nickel/ruthenium catalysts have lower activation energies than pure nickel. Besides, the $\Delta H^{\#}$ decrease after the chronoamperometry, conversely to the observed in pure nickel catalysts. The lower activation energy corresponds to $NR1800_{pc}$. The apparent activation energy for NR1800 decreases by 50% after chronoamperometry, and it is 70% lower than the activation energy of Ni_{pc} [41]. These differences in apparent activation energies may be due to the different values of activation enthalpy, found in the Conway analysis, where an increase (in absolute value) of almost 70% in the adsorption enthalpy value after ageing of the NR1800 catalyst was seen, indicating an increased tendency to adsorb water on the electrode surface.

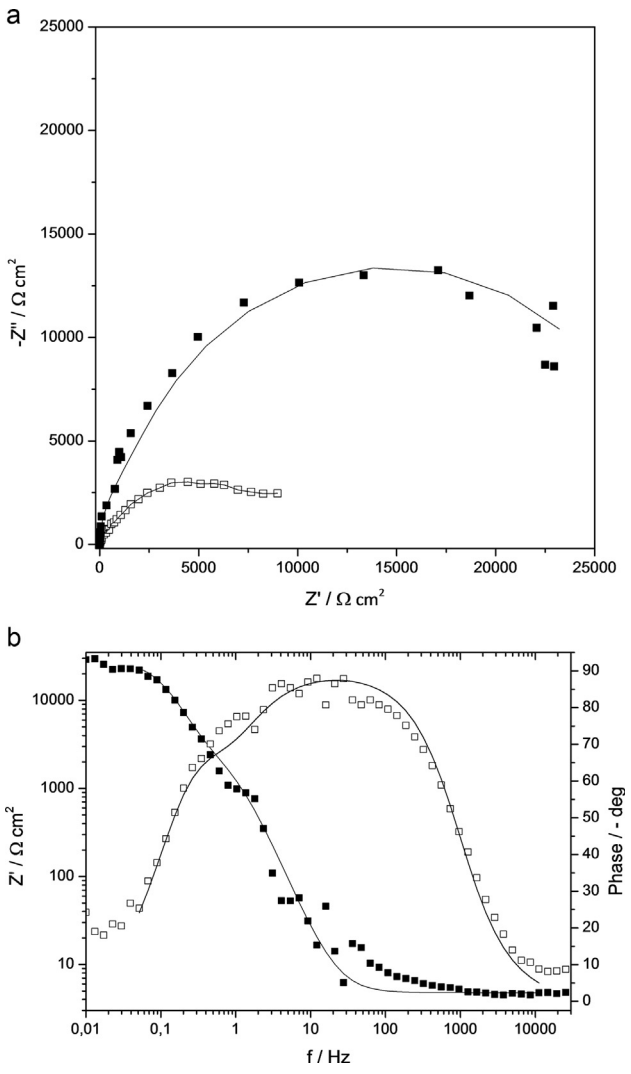

Fig. 11 – Impedance spectra in the complex plane for the HER on NR1800$_f$ (filled dots) and NR1800$_{pc}$ (open dots) in 1 M KOH at 298 K and at a rotation rate of 900 rpm, at the OCP (for each catalyst). b: Bode plot for the NR1800$_f$ catalyst in 1 M KOH at 298 K and at a rotation rate of 900 rpm at the OCP. The filled square corresponds to Z' and the open squares corresponds to the measured phase angle. The solid lines are calculated using the AHEC.

EIS

The electrochemical impedance spectra in the complex plane (Fig. 11a) recorded at the OCP (between - 0.25 V and −0.36 V), for NR500$_f$, NR1800$_f$ and NR3600$_f$ are consistent with a charge transfer controlled process [61]. Fig. 11b shows the Bode diagram corresponding to the spectra at the onset potential for NR1800$_f$ and the fit obtained using the Armstrong and Henderson equivalent circuit (AHEC) [43].

The impedance spectra in the complex plane were also determined at three values of electrode potentials, selected to cover the entire reaction region: the onset potential of HER (for each catalyst), potentials 0.1 V and 0.3 V more cathodic than the corresponding onset. Fig. 12a–c shows the impedance spectra in the complex plane for the selected potentials in the HER region. Fig. 12d shows the AHEC, where R_s is the solution resistance, R_1 is the charge transfer resistance for the electrode reaction, C_1 the double layer capacitance, R_2 is related to the superficial mass transfer resistance of H_{ad}, and C_2 is the pseudo-capacitance. In the AHEC, the Faradaic impedance, Z_f is defined as:

$$Z_f = R_1 + \frac{R_2}{1 + j\omega\tau_p} \tag{7}$$

where ω is the frequency and $\tau_p = R_2C_2$ is the time constant related to the relaxation rate when the potential is changed. The parameters obtained by fitting the data with the AHEC are shown in Table 2. These values have been normalized to the geometric area of the rotating disk electrode due to the complexity of calculating the electrochemical areas. It is well known that the formation of oxides and hydrides on the surface generates changes on its capacitance and resistance, which are hardly separable from those induced by changes in the electrochemical area [2]. In this study, the initially mirror polished electrode surfaces, maintain the polishing after the different studies, while the observed changes in the thermodynamic parameters (values of n, α_H, α_S, b, Ea) are consistent with chemical changes produced on the surface. Thus, we can assume that the differences in R and C obtained by impedance are mainly due to changes in the nature of the surface, while changes in surface area would play a minor role. For this reason we have decided to use the geometric area of the electrode as normalization parameter.

Additionally, there is a rather large dispersion in the R and C data presented in Table 2, which were obtained by fitting systematically a five components equivalent circuit. The standard deviation of the fits do not exceed 5%, so the fluctuations observed in Table 2, could be attributed to the formation of bubbles on the electrode surface which could not be removed by rotating the electrode.

There is a noticeable change in the charge transfer resistance and capacitance after the chronoamperometric pulse; this is due to the enhancement of charge transfer to generate H_{ad}. Variations in the capacitance may be associated with a change in the type of H adsorption, related with the surface hidruration.

Inserts in Fig. 12a–c shows a magnification of the Nyquist impedance spectra in the high frequency zone. It can be seen that the response, mainly in the onset potential, exhibit to linear regimes, one close to 45°, and other substantially vertical. This behavior may be related to the micro roughness of the electrode [62]. Fresh catalysts synthesized with different deposition times shows that longer deposition time is accompanied by a shift to lower frequencies of the capacitance response. A similar behavior can be observed when the aged catalysts are compared. This effect can be explained by an increase in the capacity of the electrode with deposition time, which could be related to an increased electrochemical area of the electrode but also to the presence of Ni or Ru oxides [40,63]. That is the reason why the calculation of electrochemical areas based on impedance methods for rough solid surfaces usually show a frequency dispersion which prevents the assignment of a precise value. In the case

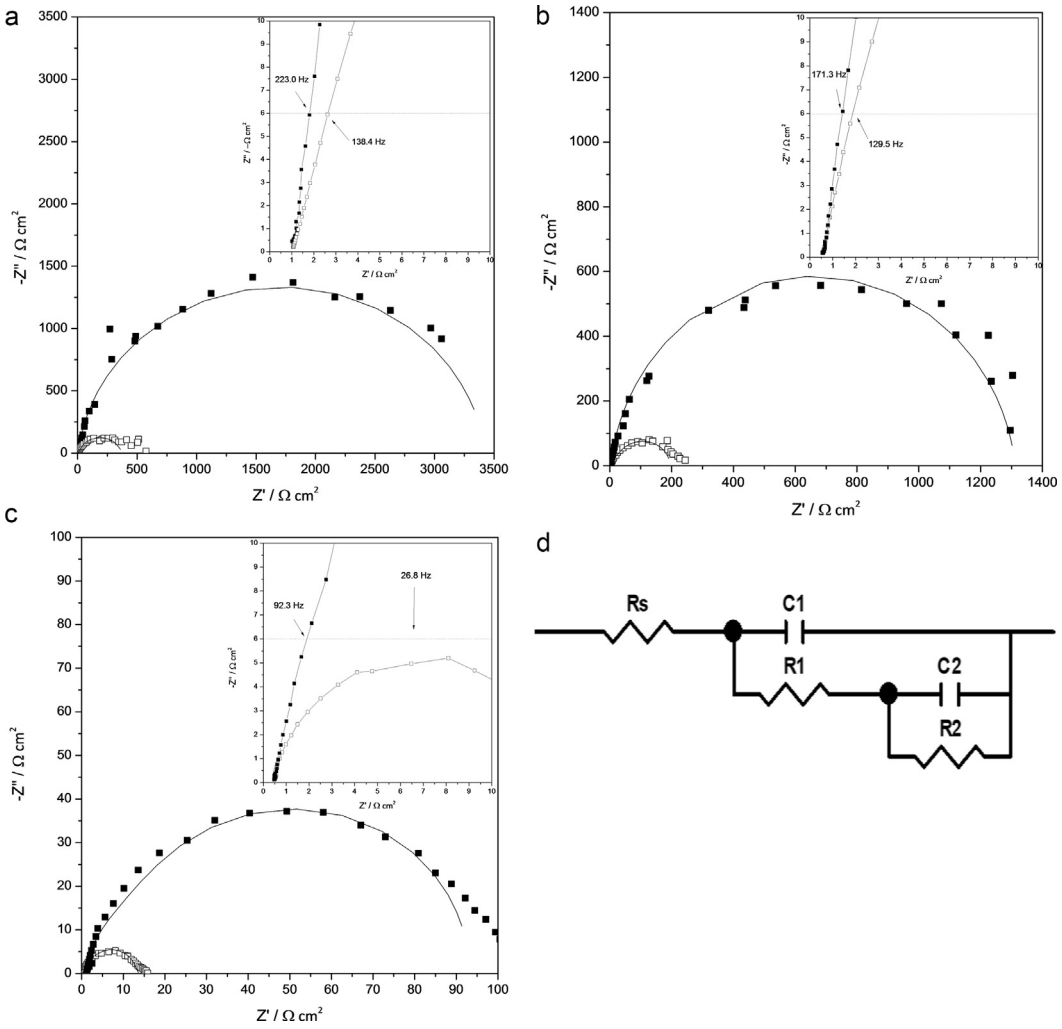

Fig. 12 – Impedance spectra in the complex plane for the HER on $NR1800_f$ (filled dots) and $NR1800_{pc}$ (open dots) in 1 M KOH at 298 K and at a rotation rate of 900 rpm, at different potentials. a) Onset potential of HER. b) overpotential 0.1 V higher that the corresponding onset potential. c) overpotential 0.3 V higher that the corresponding onset potential. d) Armstrong and Henderson equivalent electric circuit. Insert in Figures a, b, and c: Magnification of the high frequency area of the impedance spectra where the frequency correspondent to a Z″ of $-6\ \Omega cm^{-2}$ is marked.

Table 2 – Parameters of the AHEC for the HER in 1 M KOH at 298 K.

Catalyst	E (V vs SCE)	R_1 (Ω cm^2)	R_2 (Ω cm^2)	C_p (F cm^{-2})	C_{dl} (F cm^{-2})
$NR500_f$	−0.48(OCP)	6316.1	10978.5	3.35×10^{-5}	3.64×10^{-5}
	−1.04 (Onset)	243.8	3033.3	7.89×10^{-7}	2.48×10^{-5}
$NR500_{pc}$	−0.29 (OCP)	19217.9	21832.4	1.51×10^{-5}	1.33×10^{-4}
	−1.12 (Onset)	876.5	1756.7	8.14×10^{-5}	1.92×10^{-4}
$NR1800_f$	−0.24 (OCP)	9554.6	18625.7	3.37×10^{-5}	3.67×10^{-5}
	−1.02 (Onset)	1446.5	1787.1	1.22×10^{-4}	3.17×10^{-4}
$NR1800_{pc}$	−0.24 (OCP)	1143.7	6582.3	5.57×10^{-5}	2.37×10^{-4}
	−1.02 (Onset)	50.3	208.9	1.69×10^{-4}	2.08×10^{-4}
$NR3600_f$	−0.39 (OCP)	785.4	12072.2	2.57×10^{-5}	7.65×10^{-6}
	−1.14 (Onset)	1966.1	800.3	9.32×10^{-5}	6.69×10^{-4}
$NR3600_{pc}$	−0.25 (OCP)	7932.5	22837.9	3.08×10^{-5}	2.55×10^{-5}
	−1.14 (Onset)	1800.6	3191.5	1.27×10^{-4}	2.47×10^{-4}

of oxidizable transition metals, like Ni, the capacitance depends dramatically on the presence of oxide films, and the obtained electrochemical area has not a physically significant value [63].

The sum $R_1 + R_2$ (at the same potential) represents the total Faradaic resistance which is related with the kinetics of HER, and its reciprocal is directly related to the Faradaic current density. Since the HER is charge transfer controlled within the

considered potential region, the E *vs.* $\log(R_1 + R_2)^{-1}$ plot is linear, and its slope equal the Tafel slope, b. The separation observed between the conventional Tafel curves and the simulated E vs. $\log(R_1+R_2)^{-1}$ plot for all the catalysts (fresh and aged) was 1.03 ± 0.1 A cm^{-2}, close to the theoretical separation for Langmuir type adsorption [64] showing that no changes in the adsorption type can be seen after ageing, unlike what is observed in pure Ni catalysts, where after ageing Temkin type adsorption is observed.

Conclusions

In this paper the analysis of the mechanism of hydrogen evolution reaction on nickel/ruthenium electrodes is presented. The catalysts were synthesized via spontaneous deposition, by immersion of nickel electrodes in a ruthenium ions solution for different times, in order to obtain different Ru loads.

A decrease of onset potential was observed with increasing ruthenium loading up to 1800 s of deposition time, and a subsequent decrease in the catalytic activity at longer deposition times. Additionally, it was possible to observe important enhancement of the electrocatalytic activity of the nickel/ruthenium catalysts after the chronoamperometry (ageing treatment).

Some of the parameters that characterize the catalytic activity of these materials are: j_0, and the sum of R_1 and R_2 resistances related with the dj/dV slope observed in the LSV. The Ni/Ru catalysts have, after ageing, lower j_0 than that of the freshly synthesized catalysts, and that could be related to a decrease in catalytic activity. On the other hand, the decrease in the resistances R_1 and R_2, and the decrease in onset potentials enhance the catalytic activity, and these effects largely compensate the diminution of j_0. Thus, it is observed that $NR1800_{pc}$ is the catalyst with the highest electroactivity of all the electrodes examined.

The Koutecky–Levich analysis shows that there are changes in the number of electrons transferred, which increase after the short term ageing. However, the rate determining step of the reaction is the Volmer reaction, except for the NR3600 catalyst, which seems to exhibit a change in the reaction mechanism after ageing.

The results of the Tafel and EIS characterizations indicates a Langmuir type H adsorption isotherm, not only in freshly synthesized catalysts, but also in aged catalysts, unlike that observed in pure nickel, where ageing induces a Temkin type H adsorption.

Acknowledgments

The authors thank financial support from Agencia Nacional de Promoción Científica y Tecnológica, and CONICET (PIP 00095). HRC, GIL, and EAF are permanent research fellows of CONICET. The authors thank to LAMARX laboratory for its assistance in SEM/EDX measures, and to Dr. Raul Carbonio and Dra. Cecilia Blanco for XRD measurements.

Appendix A. Supplementary data

Supplementary data related to this article can be found at http://dx.doi.org/10.1016/j.ijhydene.2015.12.143.

REFERENCES

[1] Bockris JO'M, Subramanyan PK. The equivalent pressure of molecular hydrogen in cavities within metals in terms of the overpotential developed during the evolution of hydrogen. Electrochim Acta 1971;16:2169–79.
[2] Trasatti S. Progress in cathode activation. In: Gerischer H, Tobias CW, editors. Advances in electrochemical science and engineering, vol. 2. VCH Publishers; 1992. p. 1–85.
[3] Pletcher D, Xiaohong L. Prospects for alkaline zero gap water electrolysers for hydrogen production. Int J Hydrogen Energy 2011;36:15089–104.
[4] Zeng K, Zhang D. Recent progress in alkaline water electrolysis for hydrogen production and applications. Prog Energy Combust Sci 2010;36:307–26.
[5] Rausch S, Wend H. Morphology and utilization of smooth hydrogen-evolving Raney nickel cathode coatings and porous sintered-nickel cathodes. J Electrochem Soc 1996;143:2852–62.
[6] Nikolic VM, SLj Maslovara, Tasic GS, Brdaric TP, Lausevic PZ, Radak BB, et al. Kinetics of hydrogen evolution reaction in alkaline electrolysis on a Ni cathode in the presence of Ni–Co–Mo based ionic activators. Appl Catal B Environ 2015;179:88–94.
[7] Rommal HEG, Morgan PJ. The role of absorbed hydrogen on the voltage-time behavior of nickel cathodes in hydrogen evolution. J Electrochem Soc 1988;135:343–6.
[8] Soares DM, Teschke O, Torriani I. Hydride effect on the kinetics of the hydrogen evolution reaction on nickel cathodes in alkaline media. J Electrochem Soc 1992;139:98–105.
[9] Hall DS, Bock C, MacDougall BR. The electrochemistry of metallic nickel: oxides, hydroxides, hydrides and alkaline hydrogen evolution. J Electrochem Soc 2013;160:F235–43.
[10] Quaino PM, Gennero de Chialvo MR, Chialvo AC. Hydrogen electrode reaction: a complete kinetic description. Electrochim Acta 2007;52:7396–403.
[11] Losiewicz B, Budniok A, Rowinski E, Lagiewka E, Lasia A. The structure, morphology and electrochemical impedance study of the hydrogen evolution reaction on the modified nickel electrodes. Int J Hydrogen Energy 2004;29:145–57.
[12] Harrington DA, Conway BE. A.C. Impedance of faradaic reactions involving electrosorbed intermediates; Part I: kinetic theory. Electrochim Acta 1987;32:1703–12.
[13] Perez-Alonso JF, Adan C, Rojas S, Peña MA, Fierro JLG. Ni/Fe electrodes prepared by electrodeposition method over different substrates for oxygen evolution reaction in alkaline medium. Int J Hydrogen Energy 2014;39:5204–12.
[14] Tasic GS, Lacnjevac U, Tasic MM, Kaninski MM, Nikolic VM, Zugic DL, et al. Influence of electrodeposition parameters of Ni-W on Ni cathode for alkaline water electrolyser. Int J Hydrogen Energy 2013;38:4291–7.
[15] Vazquez-Gomez L, Cattarin S, Gerbasi R, Guerriero P, Musiani M. Activation of porous Ni cathodes towards hydrogen evolution by electrodeposition of Ir nuclei. J Appl Electrochem 2009;39:2165–72.
[16] Hong SH, Ahn SH, Choi I, Pyo SG, Kim HJ, Jang JH, et al. Fabrication and evaluation of nickel cobalt alloy

electrocatalysts for alkaline water splitting. Appl Surf Sci 2014;307:146–52.
[17] Tang MH, Hahn C, Klobuchar AJ, Desmond JW, Wellendorff J, Bligaard T, et al. Nickel–silver alloy electrocatalysts for hydrogen evolution and oxidation in an alkaline electrolyte. Phys Chem Chem Phys 2014;16:19250–7.
[18] Cardoso DSP, Eugenio S, Silva TM, Santos DMF, Sequeira CAC, Montemor MF. Hydrogen evolution on nanostructured Ni–Cu foams. RSC Adv 2015;5:43456–61.
[19] Aaboubi O, Ali-Omar AY, Dzoyem E, Marthe J, Boudif M. Ni-Mn based alloys as versatile catalyst for different electrochemical reactions. J Power Sources 2014;269:597–607.
[20] Santos DMF, Amaral L, Sljukic B, Macciò D, Saccone A, Sequeira CAC. Nickel-cerium electrodes for hydrogen evolution in alkaline water electrolysis. ECS Trans 2013;58:113–21.
[21] Safizadeh F, Ghali E, Houlachi G. Electrocatalysis developments for hydrogen evolution reaction in alkaline solutions – a review. Int J Hydrogen Energy 2015;40:256–74.
[22] Franceschini EA, Bruno MM, Williams FJ, Viva FA, Corti HR. High-activity mesoporous Pt/Ru catalysts for methanol oxidation. ACS Appl Mater Interfaces 2013;5:10437–44.
[23] Franceschini EA, Planes GA, Williams FJ, Soler-Illia GJAA, Corti HR. Mesoporous Pt and Pt/Ru alloy electrocatalysts for methanol oxidation. J Power Sources 2011;196:1723–9.
[24] Zhang L, Xiong K, Chen S, Li L, Deng Z, Wei Z. In situ growth of ruthenium oxide-nickel oxide nanorod arrays on nickel foam as a binder-free integrated cathode for hydrogen evolution. J Power Sources 2015;274:114–20.
[25] Guerrini E, Colombo A, Trasatti S. Surface modification of RuO_2 electrodes by laser irradiation and ion implantation: evidence of electrocatalytic effects. J Chem Sci 2009;121:639–46.
[26] Jaccaud M, Leroux F, Millet JC. New chlor-alkali activated cathodes. Mater Chem Phys 1989;22:105–19.
[27] Tavares AC, Trasatti S. Ni+RuO_2 co-deposited electrodes for hydrogen evolution. Electrochim Acta 2000;45:4195–202.
[28] Lacnjevac UC, Jovic BM, Jovic VD, Radmilovic VR, Krstajic NV. Kinetics of the hydrogen evolution reaction on Ni-(Ebonex-supported Ru) composite coatings in alkaline solution. Int J Hydrogen Energy 2013;38:10178–90.
[29] Perez-Alonso FJ, Adan C, Rojas S, Peña MA, Fierro JLG. Ni-Co electrodes prepared by electroless-plating deposition. A study of their electrocatalytic activity for the hydrogen and oxygen evolution reactions. Int J Hydrogen Energy 2015;40:51–61.
[30] Shibli SMA, Sebeelamol JN. Development of Fe_2O_3–TiO_2 mixed oxide incorporated Ni–P coating for electrocatalytic hydrogen evolution reaction. Int J Hydrogen Energy 2013;38:2271–82.
[31] Shibli SMA, Dilimon VS. Effect of phosphorous content and TiO_2-reinforcement on Ni–P electroless plates for hydrogen evolution reaction. Int J Hydrogen Energy 2007;32:1694–700.
[32] Podesta JJ, Piatt RCV, Arvia AJ, Ekdunge P, Jottner K, Kreysa G. The behavior of Ni-Co-P base amorphous alloys for water electrolysis in strongly alkaline solutions prepared through electroless deposition. Int J Hydrogen Energy 1992;17:9–22.
[33] Sankara Narayanan STN, Stephan A, Guruskanthan S. Electroless Ni–Co–B ternary alloy deposits: preparation and characteristics. Surf Coat Technol 2004;179:56–62.
[34] Schmidt T, Wendt H. Electrocatalysis of cathodic hydrogen and anodic oxygen evolution in alkaline water electrolysis by in situ activation procedures. Electrochim Acta 1994;39:1763–7.
[35] Vericat C, Wakisaka M, Haasch R, Bagus PS, Wieckowski A. Binding energy of ruthenium submonolayers deposited on a Pt (111) electrode. J Sol State Electrochem 2004;8:794–803.
[36] Crown A, Wieckowski A. Scanning tunneling microscopy investigations of ruthenium- and osmium-modified Pt(100) and Pt(110) single crystal substrates. Phys Chem Chem Phys 2001;3:3290–6.
[37] Chrzanowski W, Wieckowski A. Ultrathin films of ruthenium on low index platinum single crystal surfaces: an electrochemical study. Langmuir 1997;13:5974–8.
[38] Bianchi I, Guerrini E, Trasatti S. Electrocatalytic activation of Ni for H_2 evolution by spontaneous deposition of Ru. Chem Phys 2005;319:192–9.
[39] Vázquez-Gómez L, Cattarin S, Guerriero P, Musiani M. Influence of deposition current density on the composition and properties of electrodeposited Ni + RuO_2 and Ni + IrO_2 composites. J Electroanal Chem 2009;634:42–8.
[40] Vázquez-Gómez L, Cattarin S, Guerriero P, Musiani M. Hydrogen evolution on porous Ni cathodes modified by spontaneous deposition of Ru or Ir. Electrochim Acta 2008;53:8310–8.
[41] Franceschini EA, Lacconi GI, Corti HR. Kinetics of the hydrogen evolution on nickel in alkaline solution: new insight from rotating disk electrode and impedance spectroscopy analysis. Electrochim Acta 2015;159:210–8.
[42] Krstajic N, Popovic M, Grgur B, Vojnovic M, Sepa D. On the kinetics of the hydrogen evolution reaction on nickel in alkaline solution - part II. effect of temperature. J Electroanal Chem 2001;512:27–35.
[43] Armstrong RD, Henderson M. Impedance plane display of a reaction with an adsorbed intermediate. J Electroanal Chem 1972;39:81–90.
[44] Franceschini EA, Bruno MM, Viva FA, Williams FJ, Jobbágy M, Corti HR. Mesoporous Pt electrocatalyst for methanol tolerant cathodes of DMFC. Electrochim Acta 2012;71:173–80.
[45] Haynes WM. CRC handbook of chemistry and physics. 94th ed. Boca Raton: CRC Press; 2013.
[46] Damjanovic A. Temperature dependence of symmetry factors and the significance of experimental activation energies. J Electroanal Chem 1993;355:57–77.
[47] Rodríguez-Carvajal J. Recent advances in magnetic structure determination by neutron powder diffraction. Phys B 1993;192:55–69.
[48] Kokkinidis G, Papoutsis A, Stoychev D, Milchev A. Electroless deposition of Pt on Ti – catalytic activity for the hydrogen evolution reaction. J Electroanal Chem 2000;486:48–55.
[49] Tian D, Li DY, Wang FF, Xiao N, Liu RQ, Li N, et al. Pd-free activation method for electroless nickel deposition on copper. Surf Coat Tech 2013;228:27–33.
[50] Zhao J, Li N, Cui GF, Zhao JW. Study on immersion tin process by electrochemical methods and molecular orbital theory. J Electrochem Soc 2006;153:C848–53.
[51] Choi KH, Kim HS, Lee TH. Electrode fabrication for proton exchange membrane fuel cells by pulse electrodeposition. J Power Sources 1998;75:230–5.
[52] Tang H, Pesic B. Electrochemistry of $ErCl_3$ and morphology of erbium electrodeposits produced on Mo substrate in early stages of electrocrystallization from LiCl–KCl molten salts. Electrochim Acta 2014;133:224–32.
[53] Amin MA, Mohsen Q, Mersal GAM. Inhibition of uniform and pitting corrosion processes of Al induced by SCN- anions – Part I. Effect of glycine. Port Electrochim Acta 2010;28(2):95–112.
[54] Yussouff M. Electronic band structure and its applications. Berlin: Springer; 1987.
[55] Ashcroft NW, Mermin ND. Solid state physics. Tokyo: HRW Int. Ed. CBS Publishing Japan; 1981.
[56] Lister TE, Tolmachev YV, Chu Y, Cullen WG, You H, Yonco R, et al. Cathodic activation of RuO_2 single crystal surfaces for

hydrogen evolution reaction. J Electroanal Chem 2003;554/555:71–6.
[57] Zurilla RW, Sen RK, Yeager E. The kinetics of the oxygen reduction reaction on gold in alkaline solution. J Electrochem Soc 1978;125:1103–9.
[58] Conway BE, Tessier DF, Wilkinson DP. Temperature dependence of the Tafel slope and electrochemical barrier symmetry factor beta, in electrode kinetics. J Electroanal Chem 1989;136:2486–92.
[59] Markovic NM, Gasteiger HA, Ross PN, Jiang X, Villegas I, Weaver MJ. Electro-oxidation mechanisms of methanol and formic acid on Pt-Ru alloy surfaces. Electrochim Acta 1995;40:91–8.
[60] Goikovic SL, Vidakovic TR, Durovic DR. Kinetic study of methanol oxidation on carbon-supported PtRu electrocatalyst. Electrochim Acta 2003;48:3607–14.
[61] Krstajic N, Popovic M, Grgur B, Vojnovic M, Sepa D. On the kinetics of the hydrogen evolution reaction on nickel in alkaline solution – part I. the mechanism. J Electroanal Chem 2001;512:16–26.
[62] Huet F, Musiani M, Nogueira RP. Oxygen evolution on electrodes of different roughness: an electrochemical noise study. J Solid State Electrochem 2004;8:786–93.
[63] Trasatti S, Petrii OA. Real surface area measurements in electrochemistry. Pure Appl Chem 1991;63:711–34.
[64] Bai L, Harrington DA, Conway BE. Behaviour of overpotential-deposited species in faradaic reactions - Part II. A.C. Impedance measurements on H_2 evolution kinetics at activated and unactivated Pt cathodes. Electrochim Acta 1987;32:1713–31.